Multiple Event Triggers in Linear Covariance Analysis for Spacecraft Rendezvous

Renato Zanetti,[1] David C. Woffinden,[2] Adam Sievers,[3]
The Charles Stark Draper Laboratory, Houston, Texas, 77058

Linear covariance analysis can serve as a viable technique in determining both navigation errors and trajectory dispersions for spacecraft rendezvous analysis and design. This work addresses issues that arise when multiple events are triggered on state conditions in linear covariance analysis. To demonstrate the validity of the proposed solutions, performance metrics such as trajectory dispersions, navigation errors, delta-v dispersions, and event time dispersions are carefully analyzed and confirmed with Monte Carlo simulation results.

I. Nomenclature

$\mathbf{a}$	Acceleration
b, $\mathbf{b}$	Constant bias
$\mathbf{c}$	Compensated acceleration function
$\mathbf{C}_x$	Partial of $\mathbf{c}$ with respect to x evaluated at the nominal state
$\mathbf{D}$	Dispersions covariance
$\mathbf{e}$	Estimation error
E	Expected value
$\mathbf{E}$	Covariance of maneuver execution error
$\hat{\mathbf{g}}$	Nonlinear delta-v function from the onboard targeting algorithm

[1] Senior Member of the Technical Staff, Vehicle Dynamics and Control, 17629 El Camino Real, Suite 470, rzanetti@draper.com, Member AIAA.
[2] Senior Member of the Technical Staff, Mission Analysis and Design, 17629 El Camino Real, Suite 470, dwoffinden@draper.com, Member AIAA.
[3] First Lieutenant, US Air Force. Former Rice University Graduate Student and Draper Laboratory Fellow, 17629 El Camino Real, Suite 470, adam.sievers.1@us.af.mil, Member AIAA.

$\hat{\mathbf{G}}_x$	Partial of $\hat{\mathbf{g}}$ with respect to x evaluated at the nominal state
$\mathbf{I}$	Identity matrix
$\mathbf{J}$	Inertia matrix
$\mathbf{m}$	Nonlinear function of the change in velocity due to maneuver
$\mathbf{M}_x$	Partial of $\mathbf{m}$ with respect to x evaluated at the nominal state
n	Size of the environment state vector
$\mathbf{N}$	Matrix to map the environment state into the navigation state
$\mathbf{P}$	Estimation error covariance
$\mathbf{r}$	Position vector
$\mathbf{s}$	Constant scale factor
$\mathbf{S}$	Spectral density matrix
t	Time
$\mathbf{U}$	Event trigger reshape matrix
$\mathbf{v}$	Velocity vector
$\mathbf{V}$	Matrix with zeros everywhere except for entry corresponding to velocity states
$\mathbf{W}$	Resetting matrix
$\mathbf{x},\ \bar{\mathbf{x}},\ \hat{\mathbf{x}}$	True, nominal, and estimated state vector
$\boldsymbol{\beta}$	Markov bias
$\delta\hat{\mathbf{w}}$	Resetting uncertainty
$\delta\mathbf{x},\ \delta\hat{\mathbf{x}},\ \delta\mathbf{x}_{aug}$	Environment, navigation, and augmented dispersions
$\boldsymbol{\epsilon}$	Maneuver execution error
$\boldsymbol{\eta}$	Sensor noise
$\boldsymbol{\mu}$	Misalignment
$\boldsymbol{\upsilon}$	Inertial sensor noise
$\boldsymbol{\psi}$	Event trigger vector
$\boldsymbol{\Psi}$	Nonlinear event trigger function
$\boldsymbol{\Psi}_x$	Partial of $\boldsymbol{\Psi}$ with respect to x evaluated at the nominal state

Subscripts and Superscripts

a	Accelerometer
b	Body-fixed frame
c	Chaser vehicle or maneuver correction
e	Trigger event
g	Gyro
i	Inertial frame
imu	IMU frame
j	Covariance resetting
$lvlh$	Local Vertical Local Horizontal
m	Maneuver
rel	Relative frame
s	Covariance reshapping
st	Star tracker frame
t	Target vehicle

Symbols

$[\cdot\times]$	Function returning the cross product skew symmetric matrix
$[\cdot\diagdown]$	Function returning the diagonal matrix
$\otimes$	Quaternion multiplication

II. Introduction

When assessing the overall performance of a guidance, navigation, and control (GN&C) system, key parameters such as trajectory dispersions, navigation errors, fuel consumption, and timing of critical mission events are evaluated and analyzed. Traditionally, these performance metrics are obtained by doing hundreds or even thousands of Monte Carlo runs. Due to the complexity and the nonlinear transformations required, Monte Carlo techniques are often viewed as the only practical option. An alternative approach to Monte Carlo analysis is linear covariance analysis (LinCov) [1].

Linear covariance analysis capitalizes on linear systems theory to determine the predicted performance of a GN&C system with a single simulation run. Although linear models are ultimately required to calculate the statistical properties of the system, linear covariance analysis has a wide range of applications to non-linear systems. Recently, linear covariance analysis has taken hold in a variety of fields ranging from orbital rendezvous [2], cis-lunar [3], interplanetary missions [4], powered descent [5], and powered ascent [6]. Its potential shifted from its historic use for solely navigation analysis, to evaluating the entire closed-loop GN&C system.

The ability to capture the effects of triggering specific GN&C events such as maneuvers, sensor acquisition, or guidance mode transitions in covariance analysis framework can initially be traced back to Gossner [7] with Geller [8] providing the general formulation adopted for this research. These events can be triggered based on onboard state estimates or actual environmental conditions [3]. Initially, this capability was demonstrated for a spacecraft rendezvous and docking scenario where a single event trigger was used to initiate the final transfer maneuver. However, when this technique is extended to perform multiple event triggers for long duration rendezvous profiles, limitations may arise yielding invalid results.

The objective of this paper is to highlight the limiting factors of performing multiple event triggers for orbital rendezvous applications and provide an analytical solution to execute an arbitrary number of potential event triggers. To demonstrate and validate the proposed theoretical developments, this work provides additional contributions by 1) implementing a time state to capture the correlation and uncertainty between multiple event triggers, 2) assessing a complete rendezvous scenario with a variegate sensor suite and an assortment of targeting algorithms necessary for proximity operations, 3) formally quantifying the accuracy of linear covariance analysis for a full scale orbital rendezvous trajectory, 4) providing a simple technique to represent a reduced-state navigation filter, 5) deriving equations to utilize accelerometers in conjunction with translational maneuvers, both in the navigation filter and to determine the burn cut-off time.

III. Linear Covariance Equations

For a GN&C analysis, there are several key variables of interest which include the environment dispersions $\delta\mathbf{x}$, the navigation dispersions $\delta\hat{\mathbf{x}}$, and the navigation error $\mathbf{e}$. The environment dispersions are defined

as the difference between the environment state $\mathbf{x}$ and the nominal state $\bar{\mathbf{x}}$.

$$\delta\mathbf{x} \triangleq \mathbf{x} - \bar{\mathbf{x}} \tag{1}$$

The environment state is an $(n \times 1)$ vector that represents the true or actual state. The nominal state is also an $(n \times 1)$ vector that represents the desired or reference state such that the environment dispersions indicate how precisely the system can follow a desired trajectory. In this paper, the environment dispersions are often referred to as simply *dispersions* such that references to trajectory dispersions, inertial dispersions, relative dispersions, delta-v dispersions, or time dispersions imply the environment or true dispersions.

The navigation dispersions are defined as the difference between the navigation state $\hat{\mathbf{x}}$ and the nominal state. The navigation dispersions reflect how precisely the onboard system thinks it can follow a prescribed reference trajectory.

$$\delta\hat{\mathbf{x}} \triangleq \hat{\mathbf{x}} - \mathbf{N}\bar{\mathbf{x}}. \tag{2}$$

The navigation state is an $(\hat{n} \times 1)$ vector that represents the estimated state. The matrix $\mathbf{N}$ is an $(\hat{n} \times n)$ mapping matrix that defines the estimated state in terms of the true and nominal state. It typically *cancels* the attitude rate state when gyro measurements are incorporated in lieu of an angular rate estimate. The pseudo inverse of the matrix $\mathbf{N}$ that maps the estimated state to the true state is an $(n \times \hat{n})$ matrix $\mathbf{N}^T$.

The navigation error is the difference between the environment and navigation states. It is also the difference between the environment and the navigation dispersions. This metric characterizes how precisely the onboard navigation system can determine the actual state.

$$\mathbf{e} \triangleq \mathbf{N}\mathbf{x} - \hat{\mathbf{x}} = \mathbf{N}\delta\mathbf{x} - \delta\hat{\mathbf{x}}. \tag{3}$$

The term *error* does not necessarily reference a navigation error. For example, sensor error, control error, execution error, total error, and tracking error simply refer to the uncertainties associated with these parameters. All navigation errors are specifically referenced as either navigation errors, knowledge errors, or estimation errors.

The covariances of these variables characterize the performance of a proposed GN&C system. In a linear covariance program, this statistical information is derived by directly propagating, updating, and correcting an augmented state covariance matrix $\mathbf{D}$,

$$\mathbf{D} = E\left[\delta\mathbf{x}_{aug}\ \delta\mathbf{x}_{aug}^T\right] \tag{4}$$

where the augmented state $\delta\mathbf{x}_{aug}^{\mathrm{T}} = [\delta\mathbf{x}^{\mathrm{T}}\ \delta\hat{\mathbf{x}}^{\mathrm{T}}]$ consists of the true dispersions and the navigation dispersions. The fundamental propagation, update, and correction equations used in linear covariance analysis are available in the literature [2] and are not repeated here. This section emphasizes the particular concepts and additional developments contributed by this paper including multiple event triggers, event time dispersion calculation, the translational maneuver update with accelerometers, and the modeling of a reduced-state onboard filter.

A. Multiple Event Triggers

At orbital rates, a few seconds translate into many kilometers traveled. When an event is triggered by means other than time, there is a time delay between the nominal event time and the moment at which the event actually happens. As a result, a large dispersion between the true inertial state and the nominal state can emerge. If multiple events are initiated in a similar fashion, the dispersion in the inertial state grows larger. Conversely, as the rendezvous scenario progresses the relative dispersions and navigation errors generally become smaller. For example, during the terminal phases of rendezvous and docking, the relative navigation errors and relative trajectory dispersions can be on the order of centimeters while the inertial dispersions can be thousands of kilometers due to the implementation of multiple event triggers.

This large difference causes numerical issues when trying to compute accurate relative dispersions from the large inertial dispersions. These numerical limitations can be made less severe using square root filters [9], but fundamentally the problem remains when performing multiple event triggers. The objective of this section is to demonstrate how this short coming can be resolved for any arbitrary number of event triggers by 1) briefly summarizing a technique used for *reshaping* the augmented state covariance necessary for event triggers as discussed in [8] and [3], 2) deriving a resetting technique that will allow for an arbitrary number of potential event triggers, and 3) introducing a time state to capture the arrival time uncertainties due to performing multiple event triggers.

1. Reshaping the Augmented State Covariance Matrix

An event can be initiated based on the true state $\mathbf{x}$ such as when the spacecraft actually docks or physically enters within communication range of a target. Events can also be triggered based on the navigation state $\hat{\mathbf{x}}$ such as performing a maneuver based on the estimated elevation angle to a target spacecraft. In

general, an event trigger condition is represented as a function of either the navigation state or true state.

$$\mathbf{\Psi}\left(\mathbf{x}, \hat{\mathbf{x}}\right) = 0. \tag{5}$$

When the specified condition is achieved, it triggers a particular event that occurs at the true event time t_e. The trigger condition generally does not occur at the nominal event time $\bar{t}_e$, and the time dispersion $\delta t_e = t_e - \bar{t}_e$ can be linearly approximated as,

$$\delta t_e = \boldsymbol{\psi}_{\mathbf{x}} \delta \mathbf{x}(\bar{t}_e) + \boldsymbol{\psi}_{\hat{\mathbf{x}}} \delta \hat{\mathbf{x}}(\bar{t}_e) \tag{6}$$

where the event trigger vectors, $\boldsymbol{\psi}_{\mathbf{x}}$ and $\boldsymbol{\psi}_{\hat{\mathbf{x}}}$, are functions of the nominal state dynamics $\dot{\bar{\mathbf{x}}}$ and the event trigger partials, $\mathbf{\Psi}_{\mathbf{x}} = \frac{\partial \mathbf{\Psi}}{\partial \mathbf{x}}\big|_{\bar{\mathbf{x}}}$ and $\mathbf{\Psi}_{\hat{\mathbf{x}}} = \frac{\partial \mathbf{\Psi}}{\partial \hat{\mathbf{x}}}\big|_{\bar{\mathbf{x}}}$.

$$\boldsymbol{\psi}_{\mathbf{x}} = -\left\{\left[\mathbf{\Psi}_{\mathbf{x}} + \mathbf{\Psi}_{\hat{\mathbf{x}}}\right] \dot{\bar{\mathbf{x}}}(\bar{t}_e)\right\}^{-1} \mathbf{\Psi}_{\mathbf{x}} \tag{7}$$

$$\boldsymbol{\psi}_{\hat{\mathbf{x}}} = -\left\{\left[\mathbf{\Psi}_{\mathbf{x}} + \mathbf{\Psi}_{\hat{\mathbf{x}}}\right] \dot{\bar{\mathbf{x}}}(\bar{t}_e)\right\}^{-1} \mathbf{\Psi}_{\hat{\mathbf{x}}} \tag{8}$$

This time shift updates the true and navigation state dispersions,

$$\delta \mathbf{x}(t_e) = \delta \mathbf{x}(\bar{t}_e) + \mathbf{U}_{\mathbf{x}} \delta \mathbf{x}(\bar{t}_e) + \mathbf{U}_{\hat{\mathbf{x}}} \delta \hat{\mathbf{x}}(\bar{t}_e) \tag{9}$$

$$\delta \hat{\mathbf{x}}(t_e) = \delta \hat{\mathbf{x}}(\bar{t}_e) + \mathbf{N}\mathbf{U}_{\mathbf{x}} \delta \mathbf{x}(\bar{t}_e) + \mathbf{N}\mathbf{U}_{\hat{\mathbf{x}}} \delta \hat{\mathbf{x}}(\bar{t}_e) \tag{10}$$

and reshapes the augmented state covariance matrix to reflect the conditions triggering the event,

$$\mathbf{D}^{+s} = \begin{bmatrix} (\mathbf{I}_{\mathbf{x}} + \mathbf{U}_{\mathbf{x}}) & \mathbf{U}_{\hat{\mathbf{x}}} \\ \mathbf{N}\mathbf{U}_{\mathbf{x}} & (\mathbf{I}_{\hat{\mathbf{x}}} + \mathbf{N}\mathbf{U}_{\hat{\mathbf{x}}}) \end{bmatrix} \mathbf{D}^{-s} \begin{bmatrix} (\mathbf{I}_{\mathbf{x}} + \mathbf{U}_{\mathbf{x}}) & \mathbf{U}_{\hat{\mathbf{x}}} \\ \mathbf{N}\mathbf{U}_{\mathbf{x}} & (\mathbf{I}_{\hat{\mathbf{x}}} + \mathbf{N}\mathbf{U}_{\hat{\mathbf{x}}}) \end{bmatrix}^{\mathrm{T}} \tag{11}$$

where $\mathbf{I}_{\mathbf{x}}$ and $\mathbf{I}_{\hat{\mathbf{x}}}$ are identity matrices with a size equivalent to the true states $(n \times n)$ and navigation states $(\hat{n} \times \hat{n})$ respectively with the event trigger reshaping matrices being $\mathbf{U}_{\mathbf{x}} = \dot{\bar{\mathbf{x}}}(\bar{t}_e)\boldsymbol{\psi}_{\mathbf{x}}$ and $\mathbf{U}_{\hat{\mathbf{x}}} = \dot{\bar{\mathbf{x}}}(\bar{t}_e)\boldsymbol{\psi}_{\hat{\mathbf{x}}}$ of dimensions $(n \times n)$ and $(n \times \hat{n})$ respectively. Depending on whether the trigger is a navigation trigger or environment trigger, either $\boldsymbol{\psi}_{\mathbf{x}}$ or $\boldsymbol{\psi}_{\hat{\mathbf{x}}}$ is zero implying only $\mathbf{U}_{\mathbf{x}}$ or $\mathbf{U}_{\hat{\mathbf{x}}}$ is non-zero.

2. Resetting the Augmented State Covariance Matrix

As mentioned previously, multiple event triggers can potentially cause the inertial dispersions to become extremely large to exceed several tens of kilometers. In terms of a practical orbital rendezvous scenario, these large inertial dispersions are artificial. The nominal rendezvous trajectory is usually defined in a relative

frame, such as the local-vertical local-horizontal (LVLH) frame. Event triggers based on relative quantities, such as range or an elevation angle, exist because the nominal trajectory is a relative trajectory. While these events cause the inertial dispersions to greatly increase they reduce the relative dispersions.

Since it is the relative trajectory that is of greatest importance, the limiting numerical issues can be eliminated by simply resetting the artificial inertial dispersions. One may argue that inertial dispersions are necessary to determine lighting and beta angle constraints. In practice however, these constraints are monitored through arrival time dispersions and not the inertial location of the target. Another justification for using the resetting approach is that large inertial dispersions due to multiple event triggers could violate the linearization assumption underlying linear covariance analysis. Therefore even if these inertial dispersions were of interest, the results could be inaccurate.

The conditions governing the process of resetting the augmented state covariance matrix is as follows. The reset method must reduce the inertial dispersions without altering the relative trajectory dispersions. The reset method must also ensure the navigation errors remain unchanged, both inertial and relative navigation errors. Based on these fundamental ground rules, the resetting technique is derived by 1) introducing the approach to reset the environment dispersions without altering the navigation errors 2) developing the techniques to reset the inertial environment dispersions without affecting the relative environment dispersions and 3) derive a method to strategically reduce the inertial environment dispersions during the reset operation.

Preserving the Navigation Error In general, to reset the environment dispersions without altering the navigation errors, both the environment and navigation dispersions must be updated equally by some specified amount, $\delta\hat{\mathbf{w}}$.

$$\delta\mathbf{x}^+ = \delta\mathbf{x}^- + \mathbf{N}^T\delta\hat{\mathbf{w}} \tag{12}$$

$$\delta\hat{\mathbf{x}}^+ = \delta\hat{\mathbf{x}}^- + \delta\hat{\mathbf{w}} \tag{13}$$

To confirm this observation, substitute Eq. (12) and Eq. (13) representing the modified environment and navigation dispersions into Eq. (3) defining the navigation error. Notice that this resetting strategy does not change the navigation errors. This approach of altering both the environment and navigation dispersions equally to preserve the navigation errors serves as the basis for deriving the resetting technique for multiple event triggers for orbital rendezvous.

Preserving the Relative Trajectory Dispersions The next step is to determine the $\delta\hat{\mathbf{w}}$ that ensures the relative trajectory dispersions remain unaffected. To do so, consider the following example where the environment and navigation dispersions consist of the chaser and target inertial position and velocity dispersions

$$\delta\mathbf{x} = [\delta\mathbf{x}_c \; \delta\mathbf{x}_t] = [\delta\mathbf{r}_c \; \delta\mathbf{v}_c \; \delta\mathbf{r}_t \; \delta\mathbf{v}_t] \tag{14}$$

$$\delta\hat{\mathbf{x}} = [\delta\hat{\mathbf{x}}_c \; \delta\hat{\mathbf{x}}_t] = [\delta\hat{\mathbf{r}}_c \; \delta\hat{\mathbf{v}}_c \; \delta\hat{\mathbf{r}}_t \; \delta\hat{\mathbf{v}}_t] \tag{15}$$

such that the relative environment and navigation dispersions coordinatized in the LVLH frame can be obtained from the inertial environment and navigation dispersions,

$$\delta\mathbf{x}_{rel}^{lvlh} = \left[\delta\mathbf{r}_{rel}^{lvlh} \; \delta\mathbf{v}_{rel}^{lvlh}\right] = \mathbf{H}_{lvlh}\delta\mathbf{x} \tag{16}$$

$$\delta\hat{\mathbf{x}}_{rel}^{lvlh} = \left[\delta\hat{\mathbf{r}}_{rel}^{lvlh} \; \delta\hat{\mathbf{v}}_{rel}^{lvlh}\right] = \mathbf{H}_{lvlh}\delta\hat{\mathbf{x}} \tag{17}$$

where $\mathbf{H}_{lvlh} = \frac{\partial\hat{\mathbf{x}}_{rel}^{lvlh}}{\partial\hat{\mathbf{x}}}\Big|_{\bar{\mathbf{x}}}$ is a (6×12) matrix derived in [8]. To ensure the relative trajectory dispersions remain unchanged after the reset operation in Eqs. (12) and (13),

$$\delta\mathbf{x}_{rel}^{lvlh+} = \mathbf{H}_{lvlh}\delta\mathbf{x}^{+} = \delta\mathbf{x}_{rel}^{lvlh-} + \mathbf{H}_{lvlh}\mathbf{N}^{T}\delta\hat{\mathbf{w}} \tag{18}$$

$$\delta\hat{\mathbf{x}}_{rel}^{lvlh+} = \mathbf{H}_{lvlh}\delta\hat{\mathbf{x}}^{+} = \delta\hat{\mathbf{x}}_{rel}^{lvlh-} + \mathbf{H}_{lvlh}\delta\hat{\mathbf{w}} \tag{19}$$

the following constraint must be satisfied,

$$\mathbf{H}_{lvlh}\mathbf{N}^{T}\delta\hat{\mathbf{w}} = \mathbf{H}_{lvlh}\delta\hat{\mathbf{w}} = \mathbf{O} \tag{20}$$

where $\delta\hat{\mathbf{w}} = [\delta\hat{\mathbf{w}}_c \; \delta\hat{\mathbf{w}}_t]$ and noting that N^T equals the (12×12) identity matrix in this example.

Reducing the Inertial Trajectory Dispersions An infinite set of solutions exist for $\delta\hat{\mathbf{w}}$ that can ensure the navigation errors and relative trajectory dispersions remain unchanged following a reset. To resolve this dilemma, an additional constraint is imposed to minimize or reduce the inertial trajectory dispersions which is the primary objective of resetting the augmented state covariance.

This can be done in several ways. One option is to reset the chaser inertial dispersions to zero. Another choice is to eliminate the target inertial dispersions. An equally valid approach is to reduce both the target and chaser inertial dispersions. For this work, the target inertial navigation dispersions are reset to zero (see Eq. (13)) such that,

$$\delta\hat{\mathbf{x}}_t^{+} = \delta\hat{\mathbf{x}}_t^{-} + \delta\hat{\mathbf{w}}_t = \mathbf{0} \tag{21}$$

This implies $\delta\hat{\mathbf{w}}_t$ must equal the negative of the target inertial navigation dispersions prior to the reset operation.

$$\delta\hat{\mathbf{w}}_t = -\delta\hat{\mathbf{x}}_t^- \tag{22}$$

Given this requirement, the last step is to determine $\delta\hat{\mathbf{w}}_c$ that ensures the relative trajectory dispersions remain unchanged. Expand Eq. (20) such that it is expressed in terms of the chaser and target states, $\mathbf{H}_{lvlh} = [\mathbf{H}_c\ \mathbf{H}_t]$

$$[\mathbf{H}_c\ \mathbf{H}_t][\delta\hat{\mathbf{w}}_c^T\ \delta\hat{\mathbf{w}}_t^T]^T = \mathbf{H}_c\delta\hat{\mathbf{w}}_c + \mathbf{H}_t\delta\hat{\mathbf{w}}_t = \mathbf{O} \tag{23}$$

Substituting Eq. (22) into Eq. (23), the required expression for $\delta\hat{\mathbf{w}}_c$ emerges

$$\delta\hat{\mathbf{w}}_c = \mathbf{H}_c^{-1}\mathbf{H}_t\delta\hat{\mathbf{x}}_t^- \tag{24}$$

With Eq. (22) and Eq. (24), the updated environment and navigation dispersions in Eq. (12) and Eq. (13) can be expressed as,

$$\delta\mathbf{x}^+ = \delta\mathbf{x}^- + \mathbf{N}^T\mathbf{W}_{\hat{\mathbf{x}}}\delta\hat{\mathbf{x}}^- \tag{25}$$

$$\delta\hat{\mathbf{x}}^+ = \delta\hat{\mathbf{x}}^- + \mathbf{W}_{\hat{\mathbf{x}}}\delta\hat{\mathbf{x}}^- \tag{26}$$

where

$$\mathbf{W}_{\hat{\mathbf{x}}} = \begin{bmatrix} \mathbf{O} & \mathbf{H}_c^{-1}\mathbf{H}_t \\ \mathbf{O} & -\mathbf{I} \end{bmatrix} \tag{27}$$

The resulting equation for resetting the augmented state covariance matrix that reduces the inertial trajectory dispersions while preserving the navigation errors and the relative trajectory dispersions is,

$$\mathbf{D}^{+j} = \begin{bmatrix} \mathbf{I}_{\mathbf{x}} & \mathbf{N}^{\mathrm{T}}\mathbf{W}_{\hat{\mathbf{x}}} \\ \mathbf{NO}_{\mathbf{x}} & \mathbf{I}_{\hat{\mathbf{x}}} + \mathbf{W}_{\hat{\mathbf{x}}} \end{bmatrix} \mathbf{D}^{-j} \begin{bmatrix} \mathbf{I}_{\mathbf{x}} & \mathbf{N}^{\mathrm{T}}\mathbf{W}_{\hat{\mathbf{x}}} \\ \mathbf{NO}_{\mathbf{x}} & \mathbf{I}_{\hat{\mathbf{x}}} + \mathbf{W}_{\hat{\mathbf{x}}} \end{bmatrix}^{\mathrm{T}} \tag{28}$$

where $\mathbf{O}_{\mathbf{x}}$ is a zero square matrix with a size equal to the true state vector $\mathbf{x}$.

3. Multiple Event Time Dispersions

An analysis of arrival times is often useful in defining conditions required for a successful rendezvous. From Eq. (6), the difference between the true and nominal event times can be written in terms of the aug-

mented state $\delta\mathbf{x}_{aug}$,

$$\delta t_e = \begin{bmatrix} \boldsymbol{\psi}_{\mathbf{x}} & \boldsymbol{\psi}_{\hat{\mathbf{x}}} \end{bmatrix} \delta\mathbf{x}_{aug} \tag{29}$$

such that the variance of the particular event time is given by

$$\sigma_{t_e}^2 = \begin{bmatrix} \boldsymbol{\psi}_{\mathbf{x}} & \boldsymbol{\psi}_{\hat{\mathbf{x}}} \end{bmatrix} \mathbf{D}^{-s} \begin{bmatrix} \boldsymbol{\psi}_{\mathbf{x}} & \boldsymbol{\psi}_{\hat{\mathbf{x}}} \end{bmatrix}^{\mathrm{T}}. \tag{30}$$

This equation is useful in assessing the variation of a single event. However, when this approach is repeated for multiple events, the self-correlation of all the events is not accounted for.

In this work, the arrival time dispersion is studied by augmenting a time state to the true and navigation states, $\mathbf{x}^{\mathrm{T}} = [\mathbf{x}^{\mathrm{T}}\ t_s]$ and $\hat{\mathbf{x}}^{\mathrm{T}} = [\hat{\mathbf{x}}^{\mathrm{T}}\ \hat{t}_s]$. When an event occurs, the actual time state dispersion is updated using Eq. (9)

$$\delta t_s^+ = \mathbf{N}_{t_s}\delta\mathbf{x}^+ = \mathbf{N}_{t_s}\left[\delta\mathbf{x}^- + \mathbf{U}_{\mathbf{x}}\delta\mathbf{x}^- + \mathbf{U}_{\hat{\mathbf{x}}}\delta\hat{\mathbf{x}}^-\right] \tag{31}$$

where $\mathbf{N}_{t_s}$ is a row vector that extracts the time state dispersion. This expression in Eq. (31) can also be written in terms of the time state dynamics and the augmented state dispersions such that

$$\delta t_s^+ = \delta t_s^- + \begin{bmatrix} \dot{t}_s\boldsymbol{\psi}_{\mathbf{x}} & \dot{\hat{t}}_s\boldsymbol{\psi}_{\hat{\mathbf{x}}} \end{bmatrix} \delta\mathbf{x}_{aug}^- \tag{32}$$

Since $\frac{d}{dt}(t) = 1$ is an identity, Eq. (29) can be substituted into Eq. (32) to produce

$$\delta t_s^+ = \delta t_s^- + \delta t_e. \tag{33}$$

By augmenting the time state, the same mathematical expression for computing the arrival time dispersion is still utilized, but now the correlations between multiple events can be preserved.

B. The Translation Maneuver Update

Previous linear covariance analysis introduced translational maneuvers into the navigation filter by using a model of the thruster. For spacecraft rendezvous however, it is common to utilize accelerometers to measure the size of the maneuver. This section contains the set of equations used when the accelerometer is incorporated into the filter and i) the maneuver is executed based on a commanded on-time, and ii) the maneuver is executed based on the measured change in velocity.

Translational maneuvers directly affect the velocity states of the covariance and in particular they influence both the navigation and the true dispersions. Define $\mathbf{V}$ as a $(n \times 3)$ matrix with zeros everywhere except for a (3×3) identity matrix corresponding to the velocity states; define also $\hat{\mathbf{V}} = \mathbf{N}\,\mathbf{V}$. The maneuver updates both the environment and navigation states at t_k according to the following expressions,

$$\mathbf{x}_k^{+c} = \mathbf{x}_k^{-c} + \mathbf{V}\,\Delta\mathbf{v} \tag{34}$$

$$\hat{\mathbf{x}}_k^{+c} = \hat{\mathbf{x}}_k^{-c} + \hat{\mathbf{V}}\,\Delta\hat{\mathbf{v}} \tag{35}$$

The true velocity change $\Delta\mathbf{v}$ is a function of the execution error noise $\boldsymbol{\epsilon}_k$, the estimated state prior to the maneuver $\hat{\mathbf{x}}_k^{-c}$, and the true state prior to the maneuver $\mathbf{x}_k^{-c}$ while the estimated velocity change $\Delta\hat{\mathbf{v}}$ is derived from the compensated accelerometer measurement $\mathbf{c}\Big(\mathbf{a}, \hat{\mathbf{x}}, \mathbf{x}, \boldsymbol{\upsilon}_a\Big)$. The true inertial acceleration $\mathbf{a}$ is measured by the accelerometer in the body-fixed frame in the presence of the accelerometer noise $\boldsymbol{\upsilon}_a$ and the accelerometer error states in $\mathbf{x}$. It is compensated using the estimated accelerometer parameter states $\hat{\mathbf{x}}$ and rotated back to the inertial frame using the estimated attitude of the vehicle to propagate the vehicle dynamics. The acceleration resulting from an impulsive maneuver is modeled as a constant acceleration $\mathbf{a} = \mathbf{m}/t_m$, where t_m is the maneuver burn time such that,

$$\Delta\mathbf{v} = \mathbf{m}(\hat{\mathbf{x}}_k^{-c}, \mathbf{x}_k^{-c}, \boldsymbol{\epsilon}_k) \tag{36}$$

$$\Delta\hat{\mathbf{v}} = \mathbf{c}\Big(\mathbf{m}/t_m, \hat{\mathbf{x}}_k^{-c}, \mathbf{x}_k^{-c}, \tilde{\boldsymbol{\upsilon}}_a\Big)t_m, \tag{37}$$

where $\tilde{\boldsymbol{\upsilon}}_a$ is a zero-mean random vector with covariance $\mathbf{S}_{\upsilon_a}/t_m$. The estimated vehicle states are used to compute the commanded maneuver $\Delta\hat{\mathbf{v}}_{cmd}$. The actual maneuver is affected by the true attitude of the vehicle and the true execution parameter states which include the bias, misalignment, and scale factor terms. The environment and navigation dispersions are updated as

$$\delta\mathbf{x}_k^{+c} = \delta\mathbf{x}_k^{-c} + \mathbf{V}\,\delta\mathbf{m} \tag{38}$$

$$\delta\hat{\mathbf{x}}_k^{+c} = \delta\hat{\mathbf{x}}_k^{-c} + \hat{\mathbf{V}}\,\delta\mathbf{c} \tag{39}$$

where the perturbations of the actual maneuver $\delta\mathbf{m}$ and the compensated accelerometer measurement $\delta\mathbf{c}$ are obtained by linearizing Eq. (36) and Eq. (37) respectively

$$\delta\mathbf{m} = \mathbf{M}_{\hat{\mathbf{x}}}\delta\hat{\mathbf{x}}_k^{-c} + \mathbf{M}_{\mathbf{x}}\delta\mathbf{x}_k^{-c} + \mathbf{M}_{\boldsymbol{\epsilon}}\boldsymbol{\epsilon}_k \tag{40}$$

$$\delta\mathbf{c} = \delta\mathbf{m} + \mathbf{C}_{\hat{\mathbf{x}}}\delta\hat{\mathbf{x}}\,t_m + \mathbf{C}_{\mathbf{x}}\delta\mathbf{x}\,t_m + \mathbf{C}_{\boldsymbol{\upsilon}_a}\tilde{\boldsymbol{\upsilon}}_a t_m \tag{41}$$

The augmented dispersions are then derived by substituting Eq. (40) and Eq. (41) into Eq. (38) and Eq. (39).

$$\begin{bmatrix} \delta\mathbf{x}_k^{+c} \\ \delta\hat{\mathbf{x}}_k^{+c} \end{bmatrix} = \begin{bmatrix} \mathbf{I}+\mathbf{V}\mathbf{M}_{\mathbf{x}} & \mathbf{V}\mathbf{M}_{\hat{\mathbf{x}}} \\ \hat{\mathbf{V}}(\mathbf{C}_{\mathbf{x}}t_m+\mathbf{M}_{\mathbf{x}}) & \mathbf{I}+\hat{\mathbf{V}}(\mathbf{C}_{\hat{\mathbf{x}}}t_m+\mathbf{M}_{\hat{\mathbf{x}}}) \end{bmatrix} \begin{bmatrix} \delta\mathbf{x}_k^{-c} \\ \delta\hat{\mathbf{x}}_k^{-c} \end{bmatrix} + \begin{bmatrix} \mathbf{V}\mathbf{M}_{\boldsymbol{\epsilon}} \\ \hat{\mathbf{V}}\mathbf{M}_{\boldsymbol{\epsilon}} \end{bmatrix} \boldsymbol{\epsilon}_k + \begin{bmatrix} \mathbf{O}_{n\times 3} \\ \hat{\mathbf{V}}\mathbf{C}_{\boldsymbol{\upsilon}_a}t_m \end{bmatrix} \tilde{\boldsymbol{\upsilon}}_a$$

The covariance of the augmented state dispersion is updated due to a translational maneuver as

$$\begin{aligned} \mathbf{D}_k^{+c} = & \begin{bmatrix} \mathbf{I}+\mathbf{V}\mathbf{M}_{\mathbf{x}} & \mathbf{V}\mathbf{M}_{\hat{\mathbf{x}}} \\ \hat{\mathbf{V}}(\mathbf{C}_{\mathbf{x}}t_m+\mathbf{M}_{\mathbf{x}}) & \mathbf{I}+\hat{\mathbf{V}}(\mathbf{C}_{\hat{\mathbf{x}}}t_m+\mathbf{M}_{\hat{\mathbf{x}}}) \end{bmatrix} \mathbf{D}_k^{-c} \begin{bmatrix} \mathbf{I}+\mathbf{V}\mathbf{M}_{\hat{\mathbf{x}}} & \mathbf{V}\mathbf{M}_{\hat{\mathbf{x}}} \\ \hat{\mathbf{V}}(\mathbf{C}_{\mathbf{x}}t_m+\mathbf{M}_{\hat{\mathbf{x}}}) & \mathbf{I}+\hat{\mathbf{V}}(\mathbf{C}_{\hat{\mathbf{x}}}t_m+\mathbf{M}_{\hat{\mathbf{x}}}) \end{bmatrix}^{\mathrm{T}} \\ & + \begin{bmatrix} \mathbf{V}\mathbf{M}_{\boldsymbol{\epsilon}} \\ \hat{\mathbf{V}}\mathbf{M}_{\boldsymbol{\epsilon}} \end{bmatrix} \mathbf{E}_k \begin{bmatrix} \mathbf{V}\mathbf{M}_{\boldsymbol{\epsilon}} \\ \hat{\mathbf{V}}\mathbf{M}_{\boldsymbol{\epsilon}} \end{bmatrix}^{\mathrm{T}} + \begin{bmatrix} \mathbf{O}_{n\times 3} \\ \hat{\mathbf{V}}\mathbf{C}_{\boldsymbol{\upsilon}_a} \end{bmatrix} \mathbf{S}_{\boldsymbol{\upsilon}_a}t_m \begin{bmatrix} \mathbf{O}_{n\times 3} \\ \hat{\mathbf{V}}\mathbf{C}_{\boldsymbol{\upsilon}_a} \end{bmatrix}^{\mathrm{T}} \end{aligned} \tag{42}$$

where $\mathbf{E}_k = \mathrm{E}\left\{\boldsymbol{\epsilon}_k(\boldsymbol{\epsilon}_k)^{\mathrm{T}}\right\}$ is the maneuver execution covariance. Since $\mathbf{C}_{\hat{\mathbf{x}}} = -\mathbf{N}\,\mathbf{C}_{\mathbf{x}}$, the maneuver estimation error is given by

$$\mathbf{m} - \hat{\mathbf{m}} = \mathbf{C}_{\hat{\mathbf{x}}}\mathbf{e}\,t_m - \mathbf{C}_{\boldsymbol{\upsilon}_a}\tilde{\boldsymbol{\upsilon}}_a t_m \tag{43}$$

and the navigation covariance is updated as

$$\mathbf{P}_k^{+c} = \left(\mathbf{I}+\hat{\mathbf{V}}\hat{\mathbf{C}}_{\hat{\mathbf{x}}}t_m\right)\mathbf{P}_k^{-c}\left(\mathbf{I}+\hat{\mathbf{V}}\hat{\mathbf{C}}_{\hat{\mathbf{x}}}t_m\right)^{\mathrm{T}} + \left(\hat{\mathbf{V}}\mathbf{C}_{\boldsymbol{\upsilon}_a}\right)\mathbf{S}_{\boldsymbol{\upsilon}_a}t_m\left(\hat{\mathbf{V}}\mathbf{C}_{\boldsymbol{\upsilon}_a}\right)^{\mathrm{T}} \tag{44}$$

As expected, Eq. (44) follows directly from Eq. (42). The above equations are valid when the maneuvers are executed based on an on-time command. For example if the vehicle weighs 10,000 kg and a 200 N thruster is used to execute a 1 m/s burn, the nominal on-time t_m is 50 seconds.

When the actual execution of a maneuver is carried out using an internal closed-loop system that tracks the accelerations observed from accelerometer measurements, the maneuver is cut-off when the estimated velocity change $\Delta\hat{\mathbf{v}}$ determined by the accelerometer measurements $\mathbf{c}\Big(\Delta\mathbf{v}/t_m, \hat{\mathbf{x}}_k^{-c}, \mathbf{x}_k^{-c}, \tilde{\boldsymbol{\upsilon}}_a\Big)$ matches the commanded velocity change from the onboard targeting algorithm $\Delta\hat{\mathbf{v}}_{com} = \hat{\mathbf{g}}(\hat{\mathbf{x}})$.

$$\Delta\hat{\mathbf{v}} = \Delta\hat{\mathbf{v}}_{cmd} \tag{45}$$

$$\Delta\hat{\mathbf{v}} = \mathbf{c}\Big(\Delta\mathbf{v}/t_m, \hat{\mathbf{x}}_k^{-c}, \mathbf{x}_k^{-c}, \tilde{\boldsymbol{\upsilon}}_a\Big)t_m \tag{46}$$

By linearizing Eq. (46) and equating it to Eq. (45), the actual velocity change $\Delta\mathbf{v}$ can be expressed in terms of the commanded delta-v $\Delta\hat{\mathbf{v}}_{cmd}$ and the accelerometer measurement.

$$\Delta\mathbf{v} = \Delta\hat{\mathbf{v}}_{cmd} - \mathbf{C}_{\hat{\mathbf{x}}}\delta\hat{\mathbf{x}}_k^{-c}t_m - \mathbf{C}_{\mathbf{x}}\delta\mathbf{x}_k^{-c}t_m - \mathbf{C}_{\boldsymbol{\upsilon}_a}\tilde{\boldsymbol{\upsilon}}_a t_m \tag{47}$$

Now the update equations defined in Eq. (34) and Eq. (35) can be expressed in terms of the commanded velocity change using Eq. (47) and Eq. (45).

$$\mathbf{x}_k^{+c} = \mathbf{x}_k^{-c} + \mathbf{V}\left[\Delta\hat{\mathbf{v}}_{cmd} - \mathbf{C}_{\hat{\mathbf{x}}}\delta\hat{\mathbf{x}}_k^{-c}t_m - \mathbf{C}_{\mathbf{x}}\delta\mathbf{x}_k^{-c}t_m - \mathbf{C}_{\boldsymbol{\upsilon}_a}\tilde{\boldsymbol{\upsilon}}_a t_m\right] \tag{48}$$

$$\hat{\mathbf{x}}_k^{+c} = \hat{\mathbf{x}}_k^{-c} + \hat{\mathbf{V}}\,\Delta\hat{\mathbf{v}}_{cmd} \tag{49}$$

Noting that $\hat{\mathbf{G}}_{\hat{\mathbf{x}}} = \frac{\partial\hat{\mathbf{g}}}{\partial\hat{\mathbf{x}}}$, the change in the environment and navigation dispersions is given by

$$\begin{bmatrix}\delta\mathbf{x}_k^{+c}\\ \delta\hat{\mathbf{x}}_k^{+c}\end{bmatrix} = \begin{bmatrix}\mathbf{I}-\mathbf{V}\,\mathbf{C}_{\mathbf{x}}t_m & \mathbf{V}\left(\hat{\mathbf{G}}_{\hat{\mathbf{x}}}-\mathbf{C}_{\hat{\mathbf{x}}}t_m\right)\\ \mathbf{NO}_{\mathbf{x}} & \mathbf{I}+\hat{\mathbf{V}}\,\hat{\mathbf{G}}_{\hat{\mathbf{x}}}\end{bmatrix}\begin{bmatrix}\delta\mathbf{x}_k^{-c}\\ \delta\hat{\mathbf{x}}_k^{-c}\end{bmatrix} - \begin{bmatrix}\mathbf{V}\mathbf{C}_{\boldsymbol{\upsilon}_a}\tilde{\boldsymbol{\upsilon}}_a t_m\\ \mathbf{O}_{\hat{\mathbf{x}}}\end{bmatrix} \tag{50}$$

The updated augmented state covariance due to a translational maneuver that is executed based on compensated accelerometer measurements becomes

$$\begin{aligned}\mathbf{D}_k^{+c} = &\begin{bmatrix}\mathbf{I}-\mathbf{V}\,\mathbf{C}_{\mathbf{x}}t_m & \mathbf{V}\left(\hat{\mathbf{G}}_{\hat{\mathbf{x}}}-\mathbf{C}_{\hat{\mathbf{x}}}t_m\right)\\ \mathbf{NO}_{\mathbf{x}} & \mathbf{I}+\hat{\mathbf{V}}\,\hat{\mathbf{G}}_{\hat{\mathbf{x}}}\end{bmatrix}\mathbf{D}_k^{-c}\begin{bmatrix}\mathbf{I}-\mathbf{V}\,\mathbf{C}_{\mathbf{x}}t_m & \mathbf{V}\left(\hat{\mathbf{G}}_{\hat{\mathbf{x}}}-\mathbf{C}_{\hat{\mathbf{x}}}t_m\right)\\ \mathbf{NO}_{\mathbf{x}} & \mathbf{I}+\hat{\mathbf{V}}\,\hat{\mathbf{G}}_{\hat{\mathbf{x}}}\end{bmatrix}^{\mathrm{T}}\\ &+\begin{bmatrix}\mathbf{V}\mathbf{C}_{\boldsymbol{\upsilon}_a}\\ \mathbf{O}_{\hat{\mathbf{x}}}\end{bmatrix}\mathbf{S}_{\boldsymbol{\upsilon}_a}t_m\begin{bmatrix}\mathbf{V}\mathbf{C}_{\boldsymbol{\upsilon}_a}\\ \mathbf{O}_{\hat{\mathbf{x}}}\end{bmatrix}^{\mathrm{T}}\end{aligned} \tag{51}$$

The estimation error covariance is updated with Eq. (44).

C. Reduced-state Onboard Filter

When analyzing a GN&C system, it is common to assume a higher fidelity model for the environment than in the filter. This concept usually results in having more environment states than navigation states. The bulk of previous LinCov analysis assumes that the environment and the navigation have the same number of states (with the possible exception of angular rate in gyro replacement mode). This assumptions has one of two consequences. Either the simulation of the environment is under-conservative or the filter utilized in the analysis is overly optimistic.

When the onboard navigation filter states are the same as the true environment states, no-tuning is needed in the LinCov analysis and the only requirement is consistency between the dispersions and navigation noise parameters. In [6] a reduced order filter is used in which there are fewer navigation states than environment states. This technique has the advantage of closely matching the usual Monte Carlo analysis approach. The disadvantage is that *ad hoc* tuning is necessary in order to achieve good performance. Filter tuning is an

iterative process that denies some of the advantages of LinCov; such as obtaining quick results in a single simulation run.

A perfectly tuned reduced-order filter produces the same results as a filter considering the effects of the non-estimated states. To consider the extra states, the Schmidt-Kalman filter is used [10]. The performance of the reduced-order filter is mimicked by including all the states and simply setting to zero the rows of the Kalman gain corresponding to the non-estimated states.

IV. Orbital Rendezvous Simulation Models

The models for both the LinCov and Monte Carlo rendezvous simulations capture the translational and rotational dynamics of both a target and chaser vehicle, various sensors and actuators, and prototype GN&C algorithms. The state dynamics include the inertial position, inertial velocity, inertial-to-body attitude quaternion, and attitude rate in the body frame for both the chaser and target vehicles as well various parameter states associated with the sensors and actuators errors. The selected sensor suite includes a gyroscope, accelerometer, star tracker, light detection and ranging system (LIDAR), and global positioning system (GPS) receiver for both the chaser and target spacecraft. The torques and translational maneuvers are generated with an array of thrusters. The GN&C algorithms incorporate a dual inertial navigation filter, inertial and relative targeting algorithms, and the necessary pointing and attitude control system.

A. Dynamics

The dynamics for the chaser and target states are defined as,

$$\dot{\mathbf{r}}_c = \mathbf{v}_c \tag{52}$$

$$\dot{\mathbf{v}}_c = \mathbf{g}_c + \boldsymbol{\eta}_{a_c}\,, \quad (\mathbf{v}_c)^{+c} = (\mathbf{v}_c)^{-c} + \Delta\mathbf{v}^i \tag{53}$$

$$\dot{\bar{\mathbf{q}}}_i^c = \frac{1}{2}\,\boldsymbol{\omega}_c^c \otimes \bar{\mathbf{q}}_i^c \tag{54}$$

$$\dot{\boldsymbol{\omega}}_c^c = \mathbf{J}_c^{-1}\left[\boldsymbol{\tau}_{ctrl}^c + \boldsymbol{\tau}_g^c - \boldsymbol{\omega}_c^c \times \mathbf{J}_c\boldsymbol{\omega}_c^c\right] + \boldsymbol{\eta}_{\alpha_c} \tag{55}$$

$$\dot{\mathbf{r}}_t = \mathbf{v}_t \tag{56}$$

$$\dot{\mathbf{v}}_t = \mathbf{g}_t + \boldsymbol{\eta}_{a_t} \tag{57}$$

$$\dot{\bar{\mathbf{q}}}_i^t = \frac{1}{2}\,\boldsymbol{\omega}_t^t \otimes \bar{\mathbf{q}}_i^t \tag{58}$$

$$\dot{\boldsymbol{\omega}}_t^t = \mathbf{J}_t^{-1}\left[\boldsymbol{\tau}_g^t - \boldsymbol{\omega}_t^t \times \mathbf{J}_t\boldsymbol{\omega}_t^t\right] + \boldsymbol{\eta}_{\alpha_t} \tag{59}$$

where $\mathbf{J}_t$ and $\mathbf{J}_c$ are the target and chaser inertia matrices respectively. The accelerations due to gravity acting on the target and chaser vehicles, $\mathbf{g}_t$ and $\mathbf{g}_c$, are based on the gravity terms outlined in Table 1. The

Error Type	Variable	3σ Error	Units
Earth's gravitational constant	μ	3.986004415×10^5	$\mathrm{km}^3/\mathrm{s}^2$
Earth's equatorial radius	$R_\oplus$	6378.1363	km
Second order gravity term	J_2	1.08263×10^{-3}	
Third order gravity term	J_3	-2.56×10^{-6}	
Fourth order gravity term	J_4	-1.58×10^{-6}	

Table 1 Gravity Model Parameters

gravitational torques, $\boldsymbol{\tau}_g^t$ and $\boldsymbol{\tau}_g^c$, are derived from [11]. The control inputs, $\boldsymbol{\tau}_{ctrl}^c$ and $\Delta\mathbf{v}^i$, are the torques and impulsive velocity changes executed by the actuators on the chaser spacecraft defined in Eq. (70) and Eq. (69) respectively. The random disturbances, $\boldsymbol{\eta}_{a_t}$,$\boldsymbol{\eta}_{\alpha_t}$, $\boldsymbol{\eta}_{a_c}$, and $\boldsymbol{\eta}_{\alpha_c}$, are included in the models to account for unmodeled forces and torques acting on each spacecraft such as drag, solar radiation pressure, venting gases, etc. The uncertainty parameters for the dynamic models are summarized in Table 2.

Error Type	Variable	3σ Error	Units
Chaser unmodeled translational disturbances	$\boldsymbol{\eta}_{a_c}$	6.5727×10^{-5}	m/s/$\sqrt{s}$
Chaser unmodeled rotational disturbances	$\boldsymbol{\eta}_{\alpha_c}$	5.7500×10^{-4}	deg/s/$\sqrt{s}$
Target unmodeled translational disturbances	$\boldsymbol{\eta}_{a_t}$	6.5727×10^{-5}	m/s/$\sqrt{s}$
Target unmodeled rotational disturbances	$\boldsymbol{\eta}_{\alpha_t}$	0.0000	deg/s/$\sqrt{s}$

Table 2 State Dynamics Error Parameters

B. Sensors

The gyro model is based upon a package of three orthogonal strapdown gyros, each measuring the chaser's angular velocity along its input axis. The measured angular velocity is a function of the true angular rate $\boldsymbol{\omega}^b$ with a gyro bias $\boldsymbol{\beta}_g$, scale factor $\mathbf{s}_g$, misalignment $\boldsymbol{\mu}_g$, and the gyro angular random walk $\boldsymbol{\upsilon}_g$.

$$\tilde{\boldsymbol{\omega}}^{imu} = \mathbf{T}\left(\boldsymbol{\mu}_g\right)\left\{\mathbf{I} + [\mathbf{s}_g\diagdown]\right\}\mathbf{T}_b^{imu}\boldsymbol{\omega}^b + \boldsymbol{\beta}_g + \boldsymbol{\upsilon}_g \tag{60}$$

The gyro performance parameters are summarized in Table 3.

Error Type	Variable	3σ Error	Units
Time Constant	$\boldsymbol{\tau}_g$	3600	s
Markov Bias	$\boldsymbol{\beta}_g$	9×10^{-3}	deg/hr
Misalignment	$\boldsymbol{\mu}_g$	6	arcsec
Scale Factor	$\mathbf{s}_g$	15	ppm
Angular Random Walk	$\boldsymbol{\upsilon}_g$	7.5×10^{-3}	deg/$\sqrt{\text{hr}}$

Table 3 Gyroscope Model Error Parameters

The measured accelerations from the accelerometers are defined as the non-gravitational accelerations $\mathbf{a}^i$ plus the accelerometer bias $\boldsymbol{\beta}_a$, scale factor $\mathbf{s}_a$, misalignment $\boldsymbol{\mu}_a$, and the accelerometer random walk $\boldsymbol{\upsilon}_a$.

$$\tilde{\mathbf{a}}^{imu} = \mathbf{T}\left(\boldsymbol{\mu}_a\right)\left\{\mathbf{I} + [\mathbf{s}_a\diagdown]\right\}\mathbf{T}_b^{imu}\,\mathbf{T}_i^b\,\mathbf{a}^i + \boldsymbol{\beta}_a + \boldsymbol{\upsilon}_a \tag{61}$$

The accelerometer performance parameters are summarized in Table 4.

The star tracker provides an accurate measurement of the chaser's orientation. The generated inertial-to-star tracker quaternion is a function of the body-to-star tracker misalignment $\bar{\mathbf{q}}_{st}^b$, the actual inertial to body quaternion $\bar{\mathbf{q}}_b^i$, the sensor bias $\bar{\mathbf{q}}\left(\mathbf{b}_{st}\right)$, and noise $\bar{\mathbf{q}}\left(\boldsymbol{\eta}_{st}\right)$.

$$\tilde{\bar{\mathbf{q}}}_i^{st} = \bar{\mathbf{q}}\left(\boldsymbol{\eta}_{st}\right) \otimes \bar{\mathbf{q}}\left(\mathbf{b}_{st}\right) \otimes \bar{\mathbf{q}}(\boldsymbol{\mu}_{st}) \otimes \bar{\mathbf{q}}_b^{st} \otimes \bar{\mathbf{q}}_i^b\ , \tag{62}$$

Error Type	Variable	3σ Error	Units
Time Constant	$\boldsymbol{\tau}_a$	3600	s
Markov Bias	$\boldsymbol{\beta}_a$	30	μg
Misalignment	$\boldsymbol{\mu}_a$	15	arcsec
Scale Factor in x, y, z	$\mathbf{s}_a$	150	ppm
Velocity Random Walk	$\boldsymbol{\upsilon}_a$	30	$\mu \mathrm{g}\sqrt{\mathrm{s}}$

Table 4 Accelerometer Model Error Parameters

The star tracker parameters are summarized in Table 5.

Error Type	Variable	3σ Error	Units
Misalignment	$\boldsymbol{\mu}_{st}$	12	arcsec
Bias	$\mathbf{b}_{st}$	10	arcsec
Noise	$\boldsymbol{\eta}_{st}$		
boresignt		207	arcsec
cross boresight		49	arcsec

Table 5 Star Tracker Model Error Parameters

The chaser is equipped with a GPS receiver to update the vehicle's inertial position and velocity. The simplified GPS sensor model perturbs the actual inertial position and velocity along with bias and noise terms.

$$\tilde{\mathbf{r}}_c = \mathbf{r}_c + \boldsymbol{\beta}_{gps_r} + \boldsymbol{\eta}_{gps_r} \tag{63}$$

$$\tilde{\mathbf{v}}_c = \mathbf{v}_c + \boldsymbol{\beta}_{gps_v} + \boldsymbol{\eta}_{gps_v}. \tag{64}$$

The chaser GPS error parameters are summarized in Table 6.

The target is equipped with a GPS receiver which broadcasts the resulting inertial position and velocity measurements to the chaser spacecraft. The simplified GPS sensor model for the target vehicle is a function of the actual inertial position and velocity states along with bias and noise terms

$$\tilde{\mathbf{r}}_t = \mathbf{r}_t + \boldsymbol{\beta}_{tgps_r} + \boldsymbol{\eta}_{tgps_r} \tag{65}$$

$$\tilde{\mathbf{v}}_t = \mathbf{v}_t + \boldsymbol{\beta}_{tgps_v} + \boldsymbol{\eta}_{tgps_v}. \tag{66}$$

The target GPS performance parameters are summarized in Table 7.

Error Type	Variable	3σ Error	Units
Position Bias	$\boldsymbol{\beta}_{gps_r}$	17.3	m
Velocity Bias	$\boldsymbol{\beta}_{gps_v}$	0.173	m/s
Position Noise	$\boldsymbol{\eta}_{gps_r}$	17.3	m
Velocity Noise	$\boldsymbol{\eta}_{gps_v}$	0.173	m/s
Time Constant	τ_{gps}	300	s

Table 6 Chaser GPS Model Error Parameters

Error Type	Variable	3σ Error	Units
Position Bias	$\boldsymbol{\beta}_{tgps_r}$	90	m
Velocity Bias	$\boldsymbol{\beta}_{tgps_v}$	0.18	m/s
Position Noise	$\boldsymbol{\eta}_{tgps_r}$	90	m
Velocity Noise	$\boldsymbol{\eta}_{tgps_v}$	0.18	m/s
Time Constant	τ_{tgps}	300	s

Table 7 Target GPS Model Error Parameters

The LIDAR instrument uses laser light to directly measure the relative position between the chaser and target spacecraft. The relative position vector in the LIDAR frame is given by the equation

$$\tilde{\mathbf{r}}^l_{rel} = \mathbf{T}^l_b \mathbf{T}^b_i (\mathbf{r}_t - \mathbf{r}_c) + \mathbf{b}_{lidar} + \boldsymbol{\eta}_{lidar} \ , \tag{67}$$

where $\mathbf{r}_t$ and $\mathbf{r}_c$ are the target and chaser inertial position vectors, $\mathbf{b}_{lidar}$ is the LIDAR bias, and $\boldsymbol{\eta}_{lidar}$ is the LIDAR measurement noise. The relative position vector is used to generate the LIDAR measurements of range $\tilde{\rho}$, azimuth $\tilde{\alpha}$, and elevation $\tilde{e}$.

$$\tilde{\mathbf{r}}^l_{rel} = \begin{bmatrix} \tilde{x} \\ \tilde{y} \\ \tilde{z} \end{bmatrix} \qquad \begin{aligned} \tilde{\rho} &= \left\| \tilde{\mathbf{r}}^l_{rel} \right\|^2 \\ \tilde{\alpha} &= \arctan\left(\tilde{y}/\tilde{x}\right) \\ \tilde{e} &= \arcsin\left(\tilde{z}/\tilde{\rho}\right) \end{aligned} \tag{68}$$

The LIDAR model performance parameters are summarized in Table 8.

C. Actuators

Actuators are used to manipulate the spacecraft's translational and rotational velocities. The actual impulsive delta-v is a function of the commanded delta-v $\Delta\hat{\mathbf{v}}^i_{cmd}$ plus an associated maneuver bias $\mathbf{b}_{mvr}$,

Error Type	Variable	3σ Error	Units
Misalignment	$\boldsymbol{\epsilon}_{lidar}$	0.1	deg
Range Bias	b_ρ	0.5	m
Angles Bias	b_{az}, b_{el}	0.1	deg
Range Noise	η_ρ	0.1	m
Angles Noise	η_{az}, η_{el}	0.1	deg

Table 8 LIDAR Model Error Parameters

scale factor $\mathbf{s}_{mvr}$, misalignment $\boldsymbol{\mu}_{mvr}$, and execution noise $\boldsymbol{\eta}_{mvr}$ terms.

$$\Delta\mathbf{v}^i = \mathbf{T}_b^i\mathbf{T}\left(\boldsymbol{\mu}_{mvr}\right)\left[\left\{\mathbf{I} + \left[\mathbf{s}_{mvr}\diagdown\right]\right\}\hat{\mathbf{T}}_i^b\Delta\hat{\mathbf{v}}_{cmd}^i + \mathbf{b}_{mvr} + \boldsymbol{\eta}_{mvr}\right] \tag{69}$$

Table 9 summarizes the translational maneuver uncertainties.

Error Type	Variable	3σ Error	Units
Misalignment	$\boldsymbol{\mu}_{mvr}$	0.057	deg
Bias	$\mathbf{b}_{mvr}$	0.4	mm/s
Scale Factor	$\mathbf{s}_{mvr}$	0.495	%
Noise	η_{mvr}	0.15	mm/s

Table 9 Translational Maneuver Errors

The reaction control system (RCS) produces the torques required to alter the chaser's attitude rate. The imparted torque is modeled as a function of the commanded torque $\hat{\boldsymbol{\tau}}_{cmd}^b$ plus a torque bias $\mathbf{b}_{rot}$, scale factor $\mathbf{s}_{rot}$, misalignment $\boldsymbol{\mu}_{rot}$, and noise $\boldsymbol{\eta}_{rot}$ terms.

$$\boldsymbol{\tau}_{ctrl}^b = \mathbf{T}\left(\boldsymbol{\mu}_{rot}\right)\left[\left\{\mathbf{I} + \left[\mathbf{s}_{rot}\diagdown\right]\right\}\hat{\boldsymbol{\tau}}_{cmd}^b + \mathbf{b}_{rot} + \boldsymbol{\eta}_{rot}\right] \tag{70}$$

Table 10 summarizes the rotational maneuver uncertainties.

D. GN&C Algorithms

The prototype GN&C algorithms include a dual inertial filter for relative navigation, a PD controller to compute the commanded torques, and both relative and inertial targeting algorithms for determining the commanded impulsive maneuvers. The navigation filter estimates the inertial position and velocity of both vehicles, the attitude of the chaser spacecraft, along with the bias terms of the gyro, LIDAR, and GPS solutions.

Error Type	Variable	3σ Error	Units
Misalignment	$\boldsymbol{\mu}_{rot}$	0.057	deg
Bias	$\mathbf{b}_{rot}$	1×10^{-4}	N m
Scale Factor	$\mathbf{s}_{rot}$	1	%
Noise	$\boldsymbol{\eta}_{rot}$	3×10^{-10}	N m

Table 10 Rotational Maneuver Errors

The accelerometer is incorporated in the filter only when the sensed acceleration exceeds a predetermined threshold. The threshold is sized such that accelerometer measurements are used only during translational maneuvers. The gyroscope operates in model replacement mode where the navigation filter does not estimate angular velocity but incorporates it directly from the gyroscope measurement. The accelerometer bias and the LIDAR bias effects are considered and not estimated in the filter. The attitude PD controller for the chaser maintains the vehicle's orientation in a fixed local-vertical local-horizontal attitude. The targeting algorithms consist of a Lambert targeting algorithm[12] for rendezvous maneuvers prior to final approach and a glideslope algorithm[13] based on CW-equations for the final approach phase. Each maneuver is then executed based on the maneuver time and not the sensed accelerometer cut-off time.

V. Orbital Rendezvous Analysis

The primary objective of this orbital rendezvous analysis is to validate the theoretical developments associated with multiple event triggers in linear covariance analysis by performing an extensive comparison between solutions derived from Monte Carlo and LinCov techniques. Using similar mathematical models and error sources for the vehicle dynamics, sensors, actuators, GN&C algorithms, and disturbance accelerations and torques, the resulting trajectory dispersions, navigation errors, delta-v usage, and timing uncertainty of key mission events from each simulation tool are analyzed. A long duration rendezvous profile where multiple maneuvers are triggered based on the relative position of the chaser serves as a test scenario to validate the proposed concepts. The Monte Carlo results are based on the compilation of 1000 simulation runs which are compared to the results generated from a single LinCov simulation run utilizing the proposed resetting technique.

The basic metric to formally quantify the performance between the LinCov and Monte Carlo trajectory

dispersions and navigation errors is the *percent error difference*. The percent error difference is defined as the variation between the between the LinCov and Monte Carlo RSS value of a particular error source (i.e. relative position dispersions) divided by the RSS magnitude of the resulting Monte Carlo solution. The navigation errors are synchronized to correspond to the activation of different sensor modes. The trajectory dispersions are also synchronized to ensure they correspond to when the specific event triggers are initiated.

A. Rendezvous Mission Profile

The nominal rendezvous mission profile begins with the chaser 40 km behind a cooperating target spacecraft on a 4 km coelliptic approach trajectory with the initial condition uncertainties specified in Table 11. The target is in a circular orbit in LEO with an altitude of 350 km. When the chaser comes within 23 km of the target, it enters within communication range and the GPS data of the target vehicle is transferred to the chaser. Approximately 15 minutes after entering the vicinity to communicate with the target spacecraft, the chaser performs an orbit raising maneuver (M1) by using a lambert targeting algorithm to transfer to a specific downrange location 1.4 km below the target. This maneuver is triggered when the chaser's navigation system indicates it is 16.1 km downrange from the target. Following the successful transfer, the chaser then performs an impulsive maneuver (M2) to maintain a constant 1.4 km coelliptic approach trajectory.

Error Type	3σ Error	Units
Chaser position/velocity	20, 0.022	m, m/s
Chaser attitude/attitude-rate	5, 0.003	deg, mdeg/s
Target position/velocity	200, 0.220	m, m/s
Target attitude/attitude-rate	5, 0.003	deg, mdeg/s

Table 11 Initial Condition Errors

As the chaser coasts towards the target and reaches a downrange distance of 660 m behind the target, the terminal phase initiation (TPI) maneuver is executed. This maneuver transfers the chaser to a point 500 m below the target on the R-bar. During this R-bar acquisition phase, the LIDAR system onboard the chaser begins tracking known reflectors on the target at a range of 1.5 km but the measurements are not processed by the onboard filter until the chaser is within 600 m. Once the chaser has successfully reached the R-bar, it then performs a sequence of maneuvers known as glideslope (GS) maneuvers. These two-minute interval

burns safely bring the chaser up the R-bar to a point 20 m below the target.

The navigation architecture for the proposed rendezvous scenario utilizes relative GPS when the chaser vehicle is within communication range (23 km) but beyond 600 m. Due to potential obstructions by the target, once the chaser vehicle is 600 m below the target the primary navigation sensor switches from relative GPS to LIDAR. At this transition, the relative GPS and star tracker measurements are no longer used to compute the navigation solution and only LIDAR and IMU data are processed for the final approach phase. When available, the onboard navigation filter processes all discrete measurements every 30 seconds including star tracker, LIDAR, and GPS measurements.

B. Trajectory Dispersions

Trajectory dispersions provide significant insight into the performance a closed-loop GN&C system. They encapsulate the complex and encompassing effects of the selected sensor suite, actuator specifications, system dynamics, perturbations, initial condition uncertainty, navigation filter design, targeting logic, control algorithms, and the nominal trajectory design itself. For the proposed rendezvous scenario, Figure 1 shows both the in-plane and out-of-plane 3σ relative trajectory dispersions.

The percent difference of the total 3σ trajectory dispersions between the two analysis results is less than 4.5% near docking with a low of 0.1% during the second coelliptic coasting phase and a high of 5.4% during the transition to the second coelliptic. To highlight the strong consistency between the two analysis techniques over the entire 3.5 hour rendezvous scenario, the trajectory dispersion plot is broken down into six sub-phases in Figure 2 focusing on the initial coelliptic, the transfer to the second coelliptic, the second coelliptic approach, R-bar acquisition, glideslope, and final approach.

The effects of executing downrange event triggers for both the M1 and TPI maneuvers is apparent in the dramatic decrease in the downrange trajectory dispersions following these burns. The sharp reduction in the relative trajectory dispersions reflects the uncertainty in the chaser's relative position with respect to the occurrence of the most recent event and not the initial epoch of the simulation. As will be seen later, triggering maneuvers based on the chaser's relative position helps reduce and contain relative trajectory dispersions (and delta-v dispersions) but increases the uncertainty in the chaser's arrival time to the target.

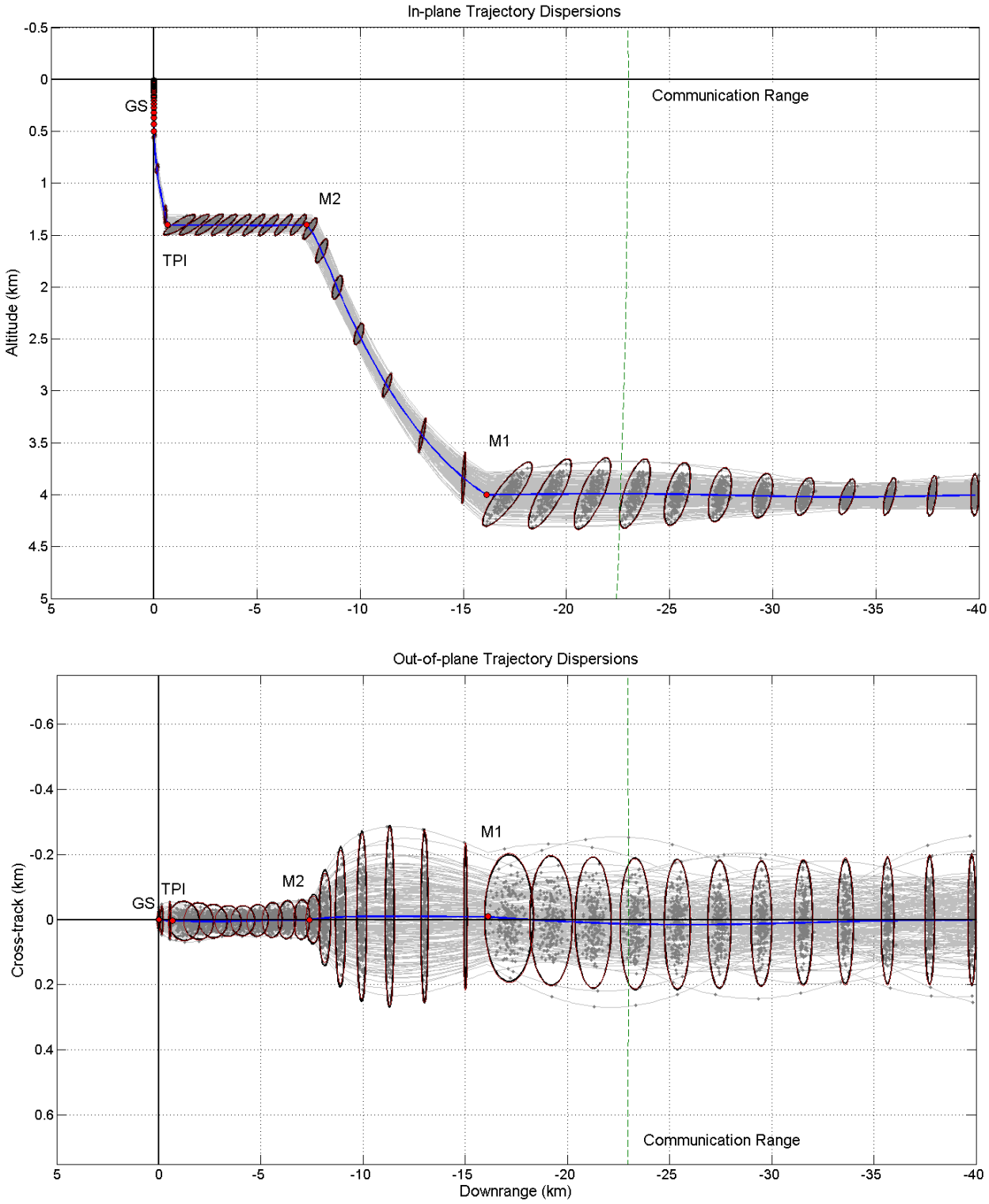

Fig. 1 Relative 3σ trajectory dispersions along the nominal trajectory in LVLH coordinates. The thick black ellipses and lines represent the statistical dispersions for 1000 Monte Carlo runs. The thick dark-colored ellipses are the dispersions derived from the LinCov analysis. The solid line passing through the center of the error ellipses represents the nominal trajectory. The first 200 sample dispersions from the Monte Carlo simulations are shown with the light gray hairlike lines and dots. Impulsive maneuvers are indicated with the solid light-colored dots.

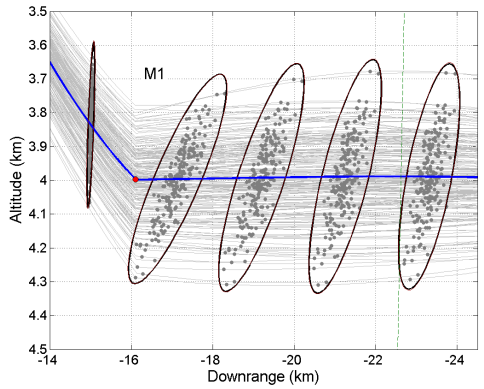

(a) First Coelliptic

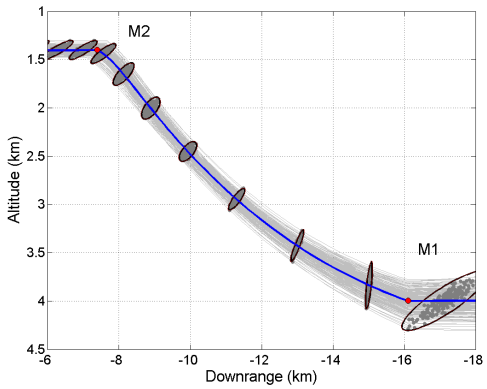

(b) Transition to Second Coelliptic

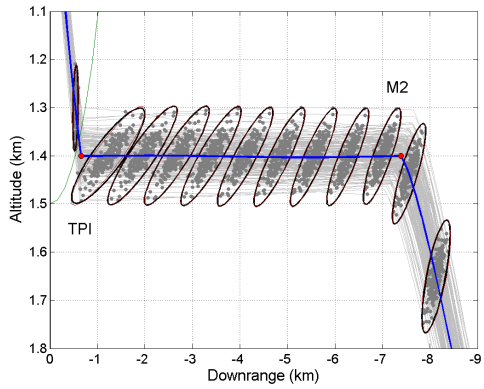

(c) Second Coelliptic

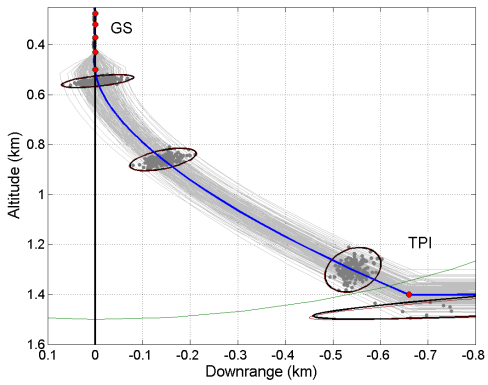

(d) R-bar Acquistion

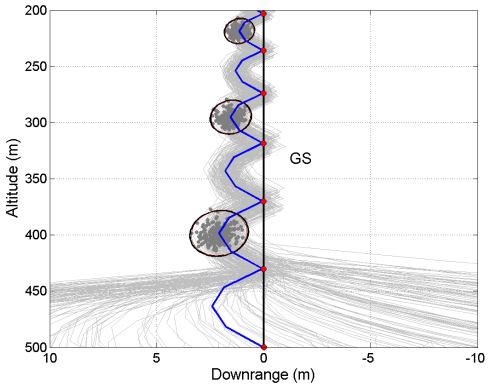

(e) Glideslope

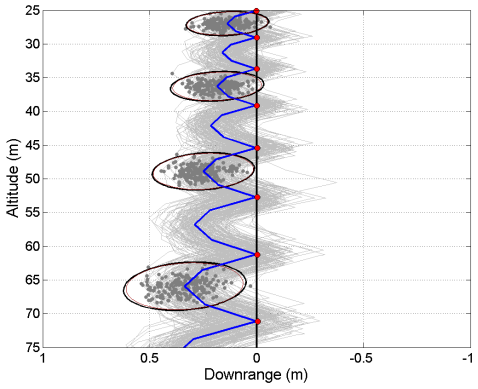

(f) Final Approach

Fig. 2 Zoom-in views of relative 3σ trajectory dispersions at specific phases in the nominal trajectory. The thick black ellipses and lines represent the statistical dispersions for 1000 Monte Carlo runs. The thick dark-colored ellipses are the dispersions derived from the LinCov analysis. The solid line passing through the center of the error ellipses represents the nominal trajectory. The first 200 sample dispersions from the Monte Carlo simulations are shown with the light gray hairlike lines and dots. Impulsive maneuvers are indicated with the solid light-colored dots.

C. Navigation Performance

When implementing the resetting technique for multiple event triggers in LinCov, the navigation performance for both the inertial and relative errors should not be affected. The objective of this section is to validate this principle by comparing the LinCov and Monte Carlo results for the chaser inertial position, target inertial position, and the relative position navigation errors. For each case, three navigation performance metrics are provided. The first is the actual or sampled navigation error derived from the 1000 Monte Carlo runs. The second is the anticipated performance computed by the navigation filter for each Monte Carlo run. The third is the predicted navigation uncertainty derived from LinCov. Recall that the LinCov navigation results are generated using a consider analysis technique that is a unique approach of representing a reduced-state navigation filter that is properly tuned. So an additional motive of this section is to also demonstrate this simple, yet effective approach for navigation analysis.

Figure 3 compares the 3σ standard deviations of chaser and target inertial position navigation error. The components of the inertial navigation errors are expressed in LVLH coordinates and are shown as a function of range. Overall, the percent difference between the LinCov and Monte Carlo predictions for the inertial chaser navigation position error is between 0.4-6.0%. The difference for the target's inertial navigation position error ranges between 0.2-4.0%. So although the resetting techniques associated with multiple event triggers alters the inertial target and chaser navigation dispersions, it still preserves the inertial navigation errors.

For rendezvous and proximity analysis, it is ultimately the relative navigation performance that is of greatest interest. Figure 4 contains the 3σ relative navigation position error plots as a function of range emphasizing the phase of flight prior to LIDAR acquisition and after LIDAR acquisition. In general, the percent difference between the two analysis approaches is within 0.2-3.5% of each other.

D. Delta V Dispersions

One elusive performance metric that has proven difficult to accurately capture in a linear covariance analysis simulation for orbital rendezvous, are the delta-v magnitude or propellant consumption dispersions. There are several possible approaches including the addition of a mass state[6]. Other adopted techniques make the assumption each maneuver is impulsive and independent from previous burns and capitalize on the

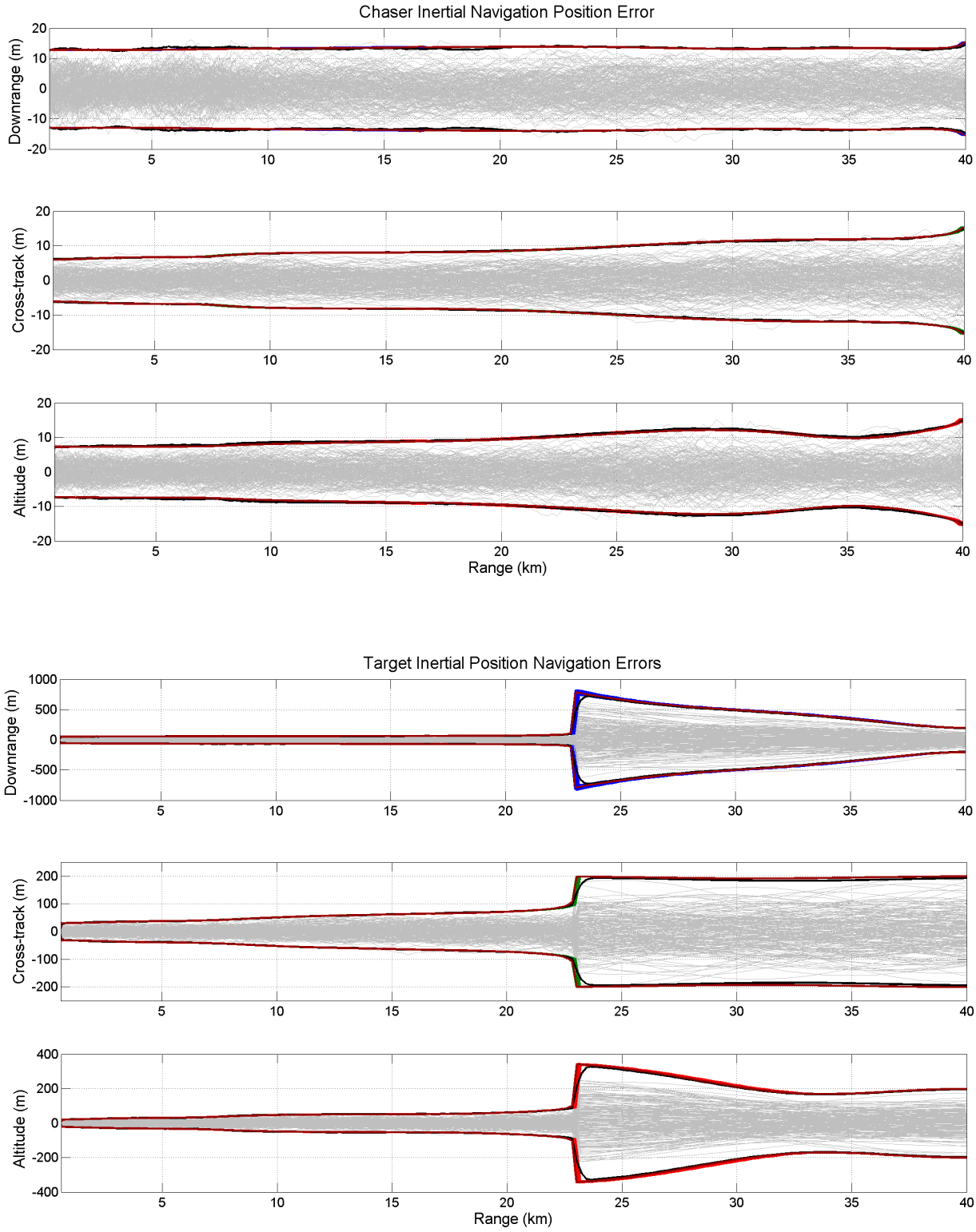

Fig. 3 Chaser and target inertial position navigation errors coordinatized in the LVLH frame. The thick black lines represent the actual 3σ navigation errors for 1000 Monte Carlo runs. The thick dark-colored lines are the 3σ navigation error bounds derived from LinCov. The thin-light colored lines are the 3σ filter navigation errors bounds. The actual navigation error from the first 200 MC simulations are shown with the light gray hairlike lines.

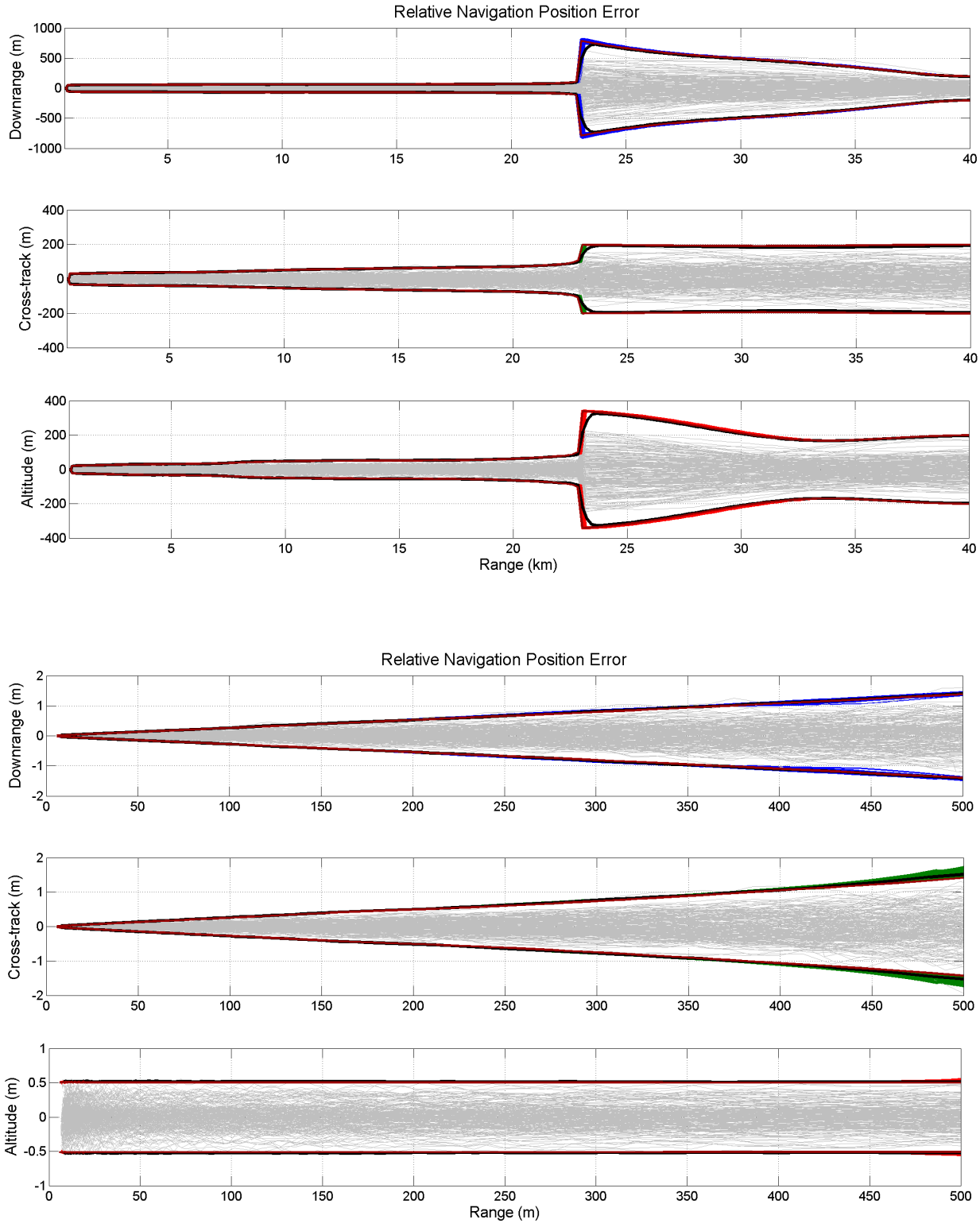

Fig. 4 Relative navigation position errors prior to LIDAR acquisition (top) and after LIDAR acquisition(bottom). The thick black lines represent the actual 3σ navigation errors for 1000 Monte Carlo runs. The thick dark-colored lines are the 3σ navigation error bounds derived from LinCov. The thin-light colored lines are the 3σ filter navigation errors bounds. The actual navigation error from the first 200 MC simulations are shown with the light gray hairlike lines.

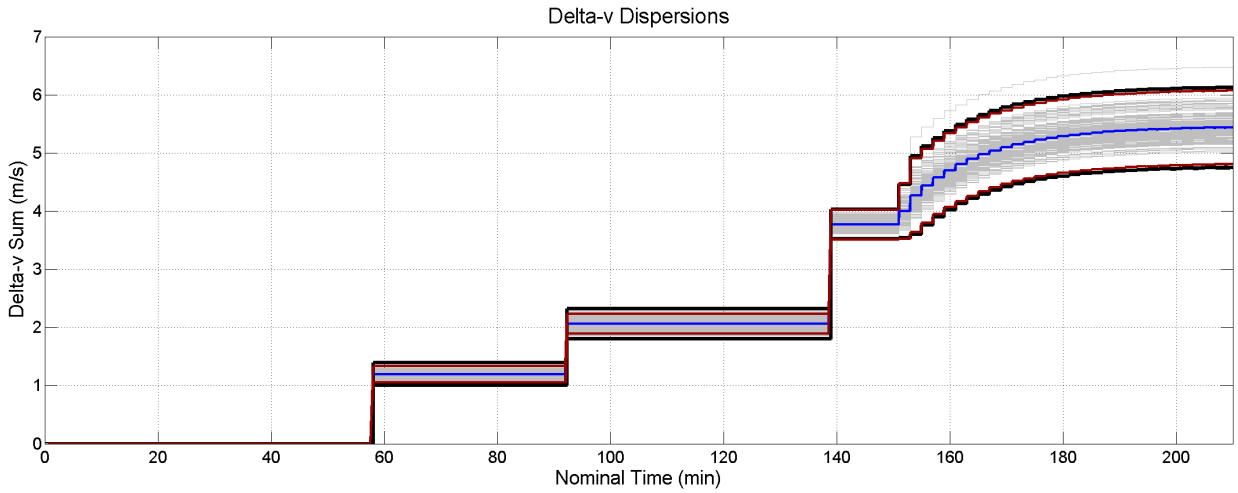

Fig. 5 Total 3σ delta-v magnitude dispersions. The thick black lines represent the 3σ statistical dispersions for 1000 Monte Carlo runs. The thick dark-colored lines are the dispersions derived from the LinCov analysis. The solid line passing through the center represents the mean (not the nominal) of the delta-v magnitude. Sample dispersions from the first 200 Monte Carlo simulations are shown with the light gray hairlike lines.

maneuver uncertainty covariance to extract the delta-v magnitude dispersions[2]. Depending on the circumstances, these options may or may not adequately capture the delta-v magnitude uncertainty. The method selected for this study numerically samples delta-v vectors as predicted from LinCov and then statistically computes the mean and standard deviation of the magnitude from the collected samples. In this fashion, there are no analytical restrictions with the non-linear transformation between the delta-v vector uncertainty and the uncertainty with its magnitude. Out of the various possibilities listed above, this technique proved to provide the most comparable results overall for this analysis.

Figure 5 shows the total delta-v magnitude for the given rendezvous scenario. Unlike previous plots, the nominal delta-v magnitude is not equivalent to the mean of the delta-v magnitude for both simulations. As a result, the trajectory dispersions are displayed with respect to the *mean* and not the nominal value. Near docking, the percent difference between LinCov and Monte Carlo delta-v dispersion prediction is 7.7%. Unlike the previous performance parameters considered, the critical delta-v information is the final mean plus 3σ value needed for delta-v budget allocation which influences the mass budget and tank sizing efforts. In terms of the final delta-v mean plus 3-sigma value, the percent difference between the two analysis techniques is 0.8%.

E. Arrival Time Dispersions

For mission critical events, it is often of interest to know the time window at which the event will take place. For rendezvous, this is particularly true for the close proximity operations to ensure proper lighting conditions and adequate time has been allocated to the mission schedule. When multiple events occur and they are correlated to one another, the challenge of accurately capturing the event time uncertainty increases.

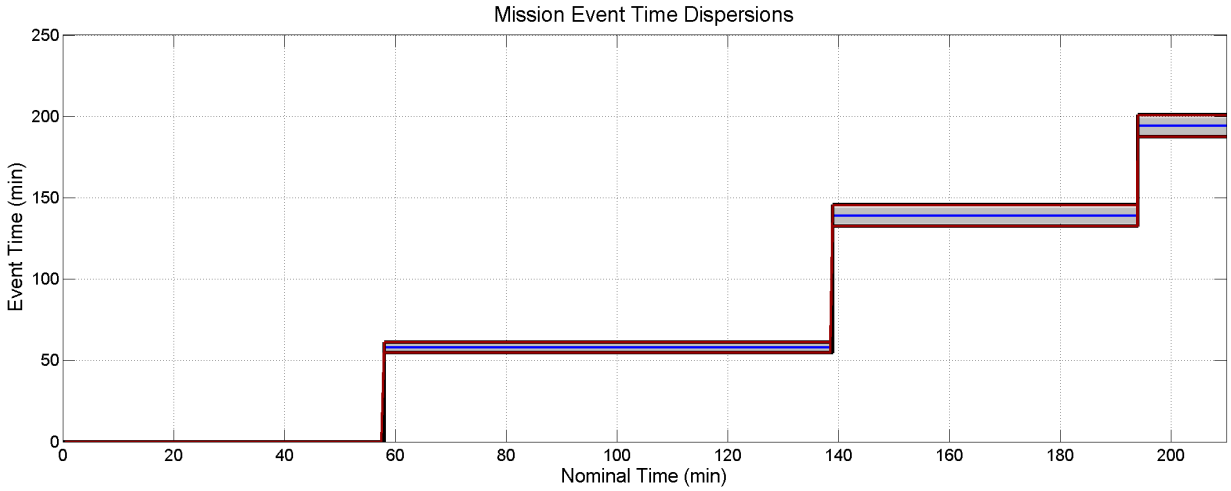

Fig. 6 The 3σ mission event time dispersions. The thick black lines represent the 3σ statistical dispersions for 1000 Monte Carlo runs. The thick dark-colored lines are the dispersions derived from the LinCov analysis. The solid line passing through the center represents the nominal event time. Sample dispersions from the first 200 Monte Carlo simulations are shown with the light gray hairlike lines.

Figure 6 shows the arrival time uncertainty for the three triggered events implemented in the proposed rendezvous scenario: the first coelliptic transfer maneuver (M1), the terminal phase initiation maneuver (TPI), and when the chaser arrives 20 m below the target. Nominally, each of these events occur at 58, 139, and 194 minutes respectively from the simulation epoch. The percent difference in the event time uncertainty between the LinCov and the Monte Carlo simulations is 0.01% for M1 and 1.7% for TPI and 1.6% at the 20 m R-bar altitude crossing. For a simulation scenario that is nominally over three hours with a final 3σ arrival time uncertainty around 6.6 minutes, the 3σ predictions by the two analysis techniques differ by 6 seconds or 0.01% for the total final arrival time prediction (nominal plus 3σ) difference.

F. Results Summary

To summarize the accuracy of implementing multiple event triggers in linear covariance analysis for orbital rendezvous, Figure 7 contains the percent difference between LinCov and Monte Carlo for the chaser and target inertial position navigation error, the relative position navigation error, and the relative trajectory dispersions for the rendezvous simulation duration. In general, the accuracy difference between the two analysis techniques is within 1-4% with periods where the precision is down to 0.1% and as large as 6% depending on the variable of interest and the mission phase. Notice that neither the relative or inertial navigation errors are affected by the proposed resetting technique. In addition, the relative trajectory dispersions remain unaffected while eliminating the numerical issues with large inertial trajectory dispersions associated with multiple event triggers.

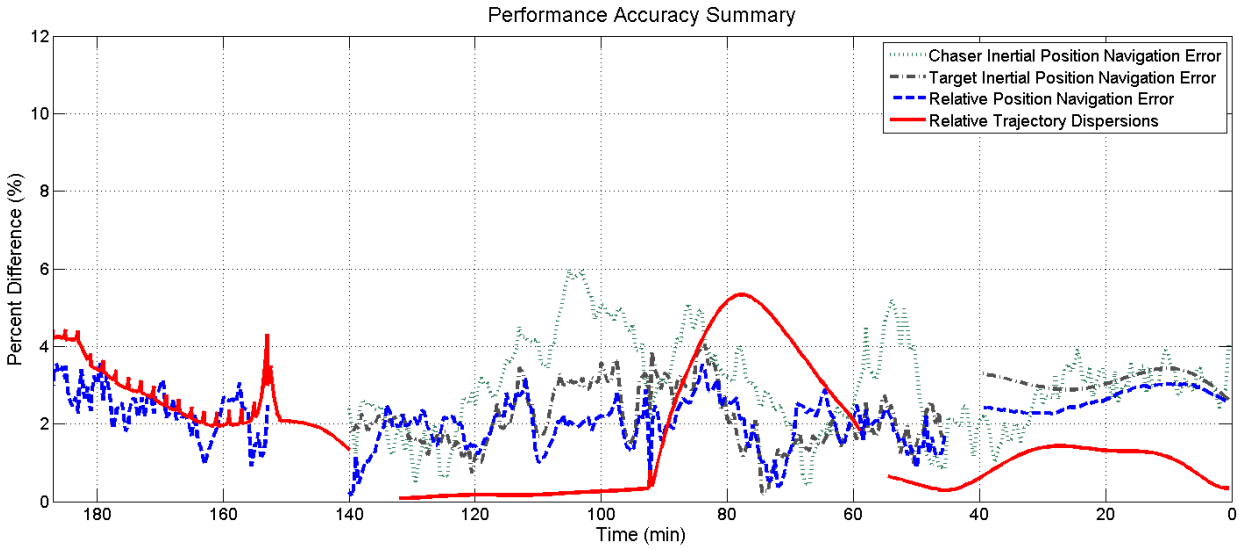

Fig. 7 Percent Accuracy between LinCov and Monte Carlo Results

Several additional comments are warranted regarding the details of Figure 7. First, the gaps in the navigation and dispersion data come from two sources; the activation of different sensors and the implementation of event triggers. For example, the percent difference of both the target inertial position and relative navigation errors is not shown over two distinct intervals. These vacant windows correspond to when the chaser reaches approximately 23 km and 600 m, the ranges both the target GPS and LIDAR measurements are activated respectively. For each Monte Carlo sample, the chaser arrives at these particular distances at different moments causing the navigation error to sharply decrease over a span of time. Instead of synchronizing the

Monte Carlo data to properly reflect the sensor acquisition periods, the sample covariance from the Monte Carlo is not calculated at these intervals resulting in the observed data gap. A similar trend is observed with the relative trajectory dispersions when the M1 and TPI maneuvers are triggered based on the chaser's down-range distance to the target. There is a brief period prior to these events where the sample covariance of the Monte Carlo data is not computed and consequently not shown.

The second point to highlight are the small spikes in the relative trajectory data towards the end of the rendezvous scenario (left side of the figure). These spikes correspond to glideslope maneuvers and are somewhat artificial due to the manner in which the sample covariance from Monte Carlo is computed. Each Monte Carlo run will perform the maneuver at a slightly different time, therefore averaging the runs will cause some of the sample to be pre-maneuver and some to be post-maneuver. As a result, there is a smoothing affect with the Monte Carlo dispersions while the LinCov results project spikes of uncertainty at the nominal maneuver times causing the minor yet noticeable discrepancy.

VI. Conclusions

Implementing event triggers in linear covariance analysis has provided a way to accurately represent transitions initiated on cues other than time. A natural by-product of this triggering strategy is an inherent uncertainty with when the event actually occurs. For orbital rendezvous applications when the spacecraft is traveling at high orbital velocities, a small time delay often translates to large dispersions in the spacecrafts inertial state. This is generally not a major concern and often goes unnoticed. So long as the relative trajectory dispersions are contained, the large inertial dispersions are not a significant factor in the mission design. However, limitations begin to arise in the linear covariance analysis framework when multiple event triggers are performed which cause the inertial dispersions to grow extremely large while significantly reducing the relative dispersions. Numerical instabilities emerge causing the linear covariance analysis results to become invalid.

This paper reveals a resetting technique that can eliminate these problems for an arbitrary number of potential event triggers for orbital rendezvous applications. The effectiveness of the resetting technique rests on several basic concepts. First, inertial dispersions for orbital rendezvous applications are inconsequential such that the limiting numerical issues can be resolved by simply resetting the artificial inertial dispersions.

Second, the resetting technique does not affect the relative or inertial navigation errors. Third, the resetting technique preserves the relative trajectory dispersions.

To demonstrate the validity of these theoretical concepts, the linear covariance analysis results are generated and compared to the sample statistics of 1000 Monte Carlo simulation runs when multiple event triggers are applied to a long duration rendezvous scenario. For a variety of GN&C performance parameters including relative trajectory dispersions, relative and inertial navigation errors, delta-v usage, and arrival time uncertainties, the LinCov and Monte Carlo results were typically within 1-4% of each other. This level of accuracy is obtained after the suite of non-linear sensor models, targeting algorithms, and flight dynamics are linearized and then implemented in the presence of environmental disturbances and initial conditions uncertainties while using multiple event triggers with the proposed resetting techniques.

In addition to establishing an analytical solution to the limitations with implementing multiple event triggers, this paper also demonstrates the effectiveness of introducing a time state to capture the correlation and arrival time uncertainty between multiple event triggers. It also formally quantifies the accuracy of a linear covariance analysis program for a full-scale rendezvous profile. In terms of navigation analysis, it provides a simple technique to represent a reduced-order filter by considering those states not included in the actual navigation filter. Lastly, it derives the basic equations to utilize accelerometers in conjunction with translational maneuvers, both in the onboard filter and for initiating burn-cut off based on accelerometer measurements.

As linear covariance techniques are applied to analyze current and future orbital rendezvous trajectories, the use of event triggers – particularly multiple event triggers – will play a natural role in the design process. The resetting method can provide a reliable solution to the limitations that multiple event triggers inherently impose. These techniques have been successfully used in the design of the Cygnus mission [14].

Acknowledgment

This work was generated under NASA contract NNJ06HC37C. The authors would like to thank Chris D'Souza for many discussions and suggestions that contributed to the ideas of this paper.

References

[1] Gelb, A., editor, *Applied Optimal Estimation*, The MIT press Massachusetts Institute of Technology, Cambridge, MA, 1974, Chapter 7.

[2] Geller, D. K., "Linear Covariance Techniques for Orbital Rendezvous Analysis and Autonomous Onboard Mission Planning," *Journal of Guidance Control and Dynamics*, Vol. 29, No. 6, November-December 2006, pp. 1404–1414.

[3] Zanetti, R., "Autonomous Midcourse Navigation for Lunar Return," *Journal of Spacecraft and Rockets*, Vol. 46, No. 4, July-Aug 2009, pp. 865–873.

[4] Stastny, N. B. and Geller, D. K., "Autonomous Optical Navigation at Jupiter: A Linear Covariance Analysis," *Journal of Spacecraft and Rockets*, Vol. 45, No. 2, Mar-Apr 2008, pp. 974–981.

[5] Geller, D. K. and Christensen, D. P., "Linear Covariance Analysis for Powered Lunar Descent and Landing," *Journal of Spacecraft and Rockets*, Vol. 46, No. 6, Nov-Dec 2009, pp. 1231–1247.

[6] Rose, M. B. and Geller, D. K., "Linear Covariance Techniques for Powered Ascent," *AIAA 2010-8175*, 2010.

[7] Gossner, J. R., *An Analytic Method of Propagating a Covariance Matrix to a Maneuver Condition for Linear Covariance Analysis During Rendezvous*, Master's thesis, Massachusetts Institute of Technology, June 1991.

[8] Geller, D. K., Rose, M. B., and Woffinden, D. C., "Event Triggers in Linear Covariance Analysis with Applications to Orbital Rendezvous," *Journal of Guidance, Control, and Dynamics*, Vol. 32, No. 1, Jan-Feb 2009, pp. 102–111.

[9] Bierman, G. J., *Factorization Methods for Discrete Sequential Estimation*, Vol. 128 of *Mathematics in Sciences and Engineering*, Academic Press, 1978, Chapter 5.

[10] Brown, G. B., Hwang, P. Y. C., *Introduction to Random Signals and Applied Kalman Filtering*, third ed., Wiley, 1997, pp. 361–367.

[11] Wertz, J. R., editor, *Spacecraft Attitude Determination and Control*, Springer, 1978, pp. 566–570.

[12] Lancaster, E. and Blanchard, R., "A Unified Form of Lambert's Theorem," Tech. rep., Goddard Space Flight Center, Greenbelt, Md., September 1969, NASA Technical Note, NASA TN D-5368.

[13] Clark, F. D., Spehar, P. T., Brazzel, J. P., and Hinkel, H. D., "Laser-Based Relative Navigation and Guidance for Space Shuttle Proximity Operations," *Proceedings of the 26th Annual AAS Guidance and Control Conference*, Breckenridge, CO, February 5–9 2003, pp. 521–529, *AAS-03-014*.

[14] Miotto, P., Breger, L., Mitchell, I., Keller, B., and Rishikof, B., "Designing and Validating Proximity Operations Rendezvous and Approach Trajectories for the Cygnus Mission," *AIAA 2010-8446*, 2010.